

# Discriminating conodont recording bias: a case study from the Nanzhang-Yuan'an Lagerstätte

Kui Wu Corresp., 1, 2, 3, Boyong Yang Corresp., 1, Bi Zhao 1, Liangzhe Yang 1, Yarui Zou 1, Gang Chen 1, Jiangli Li 1

Corresponding Authors: Kui Wu, Boyong Yang Email address: kuiwu@cug.edu.cn, boyongyang@163.com

The Early Triassic Nanzhang-Yuan´an Lagerstätte of Hubei Province, South China, preserves abundant marine reptiles in the uppermost part of the Jialingjiang Formation and provides detailed insights into marine organisms, including newly discovered and well preserved conodont clusters of the Family Ellisonidae. These conodont elements allow us to assess the bias introduced during the acquisition process. We examined conodont elements preserved on the bedding planes and those acquired after the acid-dissolving method to analyze their attributes and length distributions. We identified a biased preservation of different conodont elements related to their morphologies. After the acid-dissolving procedures, the bias increased, and all different elements were affected, with larger individuals being particularly prone to destruction. Among them, the P elements of Ellisonidae were the least affected, while the S elements were the most affected. This study further indicates that paleobiological interpretations based on fossil size or morphology could be obscured if the influence of post-mortem effect is ignored.

<sup>&</sup>lt;sup>1</sup> Hubei Institute of Geosciences, Hubei Geological Bureau, Wuhan 430034, China, Wuhan, Hubei, China

<sup>&</sup>lt;sup>2</sup> State Key Laboratory of Biogeology and Environmental Geology, School of Earth Science, China University of Geosciences (Wuhan), Wuhan 430074, China, Wuhan, Hubei, China

Hubei Key Laboratory of Resource and Ecological Environment Geology, Wuhan 430034, China, Wuhan, Hubei, China



- Discriminating conodont recording bias: a case study from
- 2 the Nanzhang-Yuan'an Lagerstätte
- 3 Kui WUa,b,c\*, Boyong YANGa\*\*, Bi ZHAOa, Liangzhe YANGa, Yarui ZOUa, Gang CHENa,
- 4 Jiangli LIa
- <sup>5</sup> <sup>a</sup> Hubei Institute of Geosciences, Hubei Geological Bureau, Wuhan, China
- 6 bState Key Laboratory of Biogeology and Environmental Geology, School of Earth Science, China
- 7 University of Geosciences (Wuhan), Wuhan, China
- 8 <sup>c</sup> Hubei Key Laboratory of Resource and Ecological Environment Geology, Wuhan, China
- 10 \*Corresponding author. E-mail: kuiwu@cug.edu.cn; \*\*Co-corresponding author.
- 11 boyongyang@tom.com
- 13 Abstract

12

14 The Early Triassic Nanzhang-Yuan'an Lagerstätte of Hubei Province, South China, preserves abundant marine reptiles in the uppermost part of the Jialingjiang Formation and 15 provides detailed insights into marine organisms, including newly discovered and well 16 preserved conodont clusters of the Family Ellisonidae. These conodont elements allow us to 17 assess the bias introduced during the acquisition process. We examined conodont elements 18 preserved on the bedding planes and those acquired after the acid-dissolving method to 19 analyze their attributes and length distributions. We identified a biased preservation of 20 different conodont elements related to their morphologies. After the acid-dissolving 21



29

30

42

procedures, the bias increased, and all different elements were affected, with larger individuals being particularly prone to destruction. Among them, the P elements of Ellisonidae were the least affected, while the S elements were the most affected. This study further indicates that paleobiological interpretations based on fossil size or morphology

26 could be obscured if the influence of post-mortem effect is ignored.

28 Keywords: Conodont; Lagerstätte; Bias; Size; Lower Triassic

1. Introduction

As nektonic marine organisms, conodont animals originated in the Cambrian and 31 disappeared near the Triassic-Jurassic boundary (Clark, 1983; Sansom et al., 1992; Goudemand et 32 33 al., 2011; Martínez-Pérez et al., 2014, 2015; Du et al., 2020). The conodont animal consists of a head, a trunk, and a caudal fin, with a feeding apparatus and two eyes attached to the head (Briggs 34 35 et al., 1983; Aldridge et al., 1993). Its total length can reach up to several centimeters or tens of 36 centimeters, while the length of a single conodont element is in the millimeter to micrometer range (e.g., Gabbott et al., 1995; Takahashi et al., 2019). Due to the absence of a mineralized skeleton, 37 conodont elements are usually the only preserved parts of conodont animals (Takahashi et al., 38 2019). Different conodont elements of an apparatus might exhibit completely different rates of 39 evolution, and rapidly evolving elements were more commonly considered and utilized for 40 biostratigraphic correlations (Orchard, 2007; Chen et al., 2016). 41

Conodont elements can be obtained in high abundance from strata though dissolution



methods, making them highly applicable and important for biostratigraphic correlations and 43 defining the geologic timescale, especially for the P<sub>1</sub> elements during the Permian-Triassic period 44 (e.g. Shen et al., 2023). To obtain sufficient conodont elements, the dissoluton method has been 45 utilized in numerous studies (e.g., Jiang et al., 2007; Sun et al., 2012), including a recent report on 46 extracting conodont elements from chert with NaOH solution (Rigo et al., 2023). For example, in 47 studies of the Permian-Triassic boundary, these methods have provided plentiful paleontological, 48 paleoenvironmental, and biostratigraphic information, greatly improving our understanding of the 49 geological processes during this interval (Sun et al., 2012; Chen et al., 2013; Dal Corso et al., 2022; 50 51 Shen et al., 2023). Conversely, due to limitations related to their size, morphology, preservation condition and preparation methods, fewer apparatuses or clusters have been found directly on the 52 rock surface. However, more details about the conodont animal have been revealed through to 53 54 these materials (e.g., Gabbott et al., 1995; Goudemand et al., 2011; Sun et al., 2020). We have known since the last century that the fossil record of conodonts can be fundamentally 55 biased due to taphonomic processes and laboratory procedures (Purnell and Donoghue, 2005; von 56 Bitter and Purnell, 2005). First of all, the preservation of conodont elements in the strata is 57 influenced by their morphology, which may lead to biased fossilization of different anatomical 58 units (Purnell and Donoghue, 2005; Orchard, 2007). Additionally, the differential destruction of 59 elements during laboratory processes, particularly the acid-dissolving method, affects conodont 60 data, including the numbers, dimensions (reducing size by breakage), and ratios of different 61 conodont elements (von Bitter, 1972; Jeppsson and Anehus, 1995; von Bitter and Purnell, 2005). 62 For example, the apparatus of Ellisonidae consists of 4 P elements, 2 M elements and 9 S elements 63



(Sun et al., 2020), while results after laboratory processes exhibited variable ratios of different 64 elements (Koike, 2016; also see summary in the supplementary file of this study). Furthermore, 65 previous studies have shown that the size of the conodont element is not only related to ecological 66 change but also to taxonomic identification (Chen et al., 2013; Chen et al., 2016; Ginot and 67 Goudemand, 2019). Hence, this basic biological trait of conodont elements has been largely 68 69 investigated, although the impact of laboratory processes on conodonts size is usually not mentioned (e.g. Chen et al., 2013; Wu et al., 2019; Zhang et al., 2020; Leu et al., 2019). 70 Specifically, as one of the three main Early Triassic conodont groups, the ellisonids have been less 71 recognized and understood compared to the anchignathodontids and gondolellids, and they were 72 thought to have suffered an extinction at the Smithian-Spathian boundary (Orchard, 2007). A 73 recent study showed that large amounts of ellisonids were preserved in the uppermost Lower 74 Triassic of Hubei Province, South China, suggesting that the Early Triassic records of ellisonids 75 have been obscured by their special morphology as well as laboratory processes (Wu et al., 2023). 76 77 As one of the most famous areas for Early Triassic marine organisms, abundant and well-78 preserved fossil specimens have been found in the limestone of the uppermost Jialingjiang 79 Formation in the Nanzhang-Yuan'an area (Wu et al., 2023), making it a fossil-Lagerstätte for the latest Early Triassic geologic record in South China (Benton et al., 2013; Kimming and 80 Schiffbauer, 2024). Hence, this Lagerstätte provides an invaluable opportunity to fully investigate 81 the organisms and address biases encountered when interpreting the fossil details of conodonts 82 from the geological records. Recently, abundant conodont elements of Ellisoniidae have been 83 discovered in this section (Wu et al., 2023). Our study further contributes to this research by 84



Associations of conodonts on the bedding planes serve as the most reliable archive for biological traits, unaffected by laboratory treatment (Goudemand et al., 2012; Sun et al., 2020). Through quantitative analysis of composition, size, and ratio of different elements, this study offers the opportunity to examine biases originating from both the bedding planes and the residues after the acid-dissolving method, with implications for other types of conodonts during the Early Triassic.

#### 2. Location and geological setting

The studied Zhangjiawan section is about 25 km north of Yuan'an County, in the western part of Hubei Province, south-central China (Wu et al., 2023). During the Early Triassic, the South China block was located near the equator in the eastern part of the Tethys Ocean, while extensive shallow-marine deposits recorded in the North Marginal Basin of the Yangtze Platform (see Fig.1 of Wu et al., 2023). To date, numerous fish fossils have been reported from the Lower Triassic of the North Marginal Basin, and two distinctive marine reptile faunas (the Nanzhang-Yuan'an fauna and the Chaohu fauna) have also been found from this region (Benton et al., 2013).

As a representative section of the Nanzhang-Yuan'an fauna, the Zhangjiawan section is well-exposed along a road and a quarry, with a thickness of approximately 120 m (Wu et al., 2023). The section outcrops vermicular limestone, limestone, dolomite, brecciated dolomite, laminated limestone, volcanic tuffs, and sandy mudstone, indicating that it belongs to the restricted platform facies (Wu et al., 2023). Reported marine reptiles were all found in the laminated limestone, which is about 36 meters thick. A 0.5-meter-thick unit of wedge-like or lenticular-like strata, consisting



of centimeter-sized thin beds, appear in the middle part of the laminated limestone (Fig. 1A), suggesting the deepest depositional environment with minimal hydrodynamic effect in this section. Recent studies have shown that the Nanzhang-Yuan'an fauna was extensively and well documented in this region, making it one of the youngest Early Triassic Lagerstätte for marginal sea animals, particularly those with hard skeletons (Yan et al., 2021; Wu et al., 2023; Kimming and Schiffbauer, 2024).

#### 3. Materials and method

The materials from the bedding planes were found through systematical collection rather than incidental discovery. Bulk samples, each weighing approximately 5 kg, were initially collected from the Zhangjiawan section (Wu et al., 2023). These samples were then crushed into pieces measuring around 3×3 cm (sometimes lager) and processed with 10% diluted acetic acid. A conodont cluster was obtained from the residues after the acetic acid dissolving and sieve-separating procedures (Fig. 1B), indicating that well-preserved clusters may have been preserved on the bedding planes, which were millimeters in thickness.

The sample containing conodont clusters was taken from the middle part of the dark-colored lamellar limestone, which is the thinnest bed in the Zhangjiawan section. Consequently, approximately 30 kg of cracked rocks were collected from this bed and observed directly under a binocular microscope. For better comparison, a sample weighing about 20 kg was collected from the location where the cluster was found. This sample consisted of limestone laminae, millimeters in thickness. To avoid crushing, which might destroy conodont elements, these limestone laminae



128

129

130

131

132

133

134

135

136

137

138

139

140

141

142

143

144

145

146

147

were processed directly with 10% diluted acetic acid. The sample was kept in the diluted acetic acid for about 24 hours until only minor or no bubble were visible. The supernatant liquid was then poured out, and fresh diluted acetic acid was added. Every 5 days thereafter, the undissolved residues were sieved using 20-mesh (0.850 mm, on top) and 160-mesh (0.095 mm, on bottom) sieves. This process continued until all the rocks were dissolved. After drying the residues in an oven at 30°C, they were examined under a binocular stereo-microscope to obtain conodont elements. The lengths of conodont elements from the bedding planes and those obtained through the acetic acid dissolving method (including both complete and broken elements) were measured in microns. Following the common practice in size studies (Wu et al., 2019; Baets et al., 2022), all data were also logarithmized (base 10) for statistical analysis. Due to their prominent cusp and the presence of the third process. Ellisonidae elements exhibite more variable morphology than other Early Triassic conodonts (Orchard, 2007). According to anatomical standards and morphological aspects, conodont elements were classified into three types: P, M, and S elements (Purnell et al., 2000; Sun et al., 2020). For M elements, the distance from the tip of the cusp to the distal end of the longer process was measured (Fig. 1C). For P and S elements with only one process, the distance between the two distal ends was measured (Fig. 1D-G, I-L). For those elements with three

preserved on rock surfaces, further classification into P  $(P_{1-2})$  and S  $(S_{0-4})$  elements was not



considered in this study. To make a better comparison, multielement composition data of various Ellisonidae species from Koike (2016) were also collected.

#### 4. Results

Due to the low abundance of conodonts from the upper Lower Triassic, particularly from the Jialingjiang Formation of South China (Zhao et al., 2013; Wu et al., 2023), a total of 167 and 71 conodont elements (including both broken and complete elements) were acquired from the bedding planes and the residues after acid-dissolving, respectively (Table 1). The conodonts from the bedding planes comprised 25 P elements (14.97%), 21 M elements (12.57%) and 121 S elements (72.46%) (Fig. 2A). In contrast, the residues after acid-dissolving yielded 17 P elements (23.94%), 17 M elements (23.94%) and 37 S elements (52.11%) (Fig. 2A), indicating that the latter method resulted in fewer acquisitions of all element types. Compared with the standard composition of the Ellisonidae apparatus, M elements obtained from the acid-dissolution method and S elements preserved on the bedding planes exhibit an increase of the ratio (Fig. 2B). A comparison with the data from Koike (2016) suggests that results could be influenced differently due to their varying morphologies, even within the same species from different samples (Fig. 3).

Percentages of complete and broken conodont elements from the bedding planes and the acid-dissolving method were also different (Fig. 4). For the conodonts preserved on the bedding planes, complete elements comprised 21 P elements (84.00%), 6 M elements (28.57%), and 89 S elements (73.55%). In contrast, for the conodonts obtained from the acid-dissolution method, complete elements comprised of 8 P elements (47.06%), 11 M elements (67.71%), and 12 S elements



169 (32.43%).

Despite the lower yield, the two groups of conodonts exhibit noticeable differences (Table 1; 170 Figure 5 and 6). The average lengths of the conodont elements from the bedding planes and 171 residues are 948.4 µm and 700.7 µm, respectively, with standard deviation of 430.6 and 228.5. 172 This suggests that conodont elements from bedding planes seem generally larger. For the conodont 173 174 elements preserved on the bedding planes (Table 1), P elements range in length from 450 µm to 1550 μm, with an average of 868.4 μm and a standard deviation of 331.6 μm. M elements range 175 from 240 µm to 1600 µm, with an average of 747.4 µm and a standard deviation of 337.9 µm. S 176 elements range from 290 µm to 2810 µm, with an average of 999.9 µm and a standard deviation 177 of 449.8 µm. For the conodont elements obtained from the residues after acid-dissolving (Table 178 1), P elements range in length from 447 µm to 1226 µm, with an average of 753.8 µm and a 179 standard deviation of 190.4 µm. M elements range from 341 µm to 1345 µm, with an average of 180 680.8 μm and a standard deviation of 254.9 μm. S element range from 356 μm to 1373 μm, with 181 an average of 685.5 µm and a standard deviation of 227.8 µm. A two-sample t-test indicates that 182 the sizes of P and M elements from different methods are not highly significantly different in size 183 (p=0.51 and 0.21, respectively), although those from the bedding planes are generally larger. In 184 contrast, S elements from the two groups show a highly significant size difference (p < 0.01). 185 Considering all elements of different types from each group, they exhibit significantly different 186 length distributions. A percentile plot reveals that S elements from the bedding planes include 187 noticeable larger individuals, whereas the other types have similar length distribution percentages. 188 Over all, conodont elements from the bedding planes tend to be larger and have a higher percentage 189



of S elements (Fig. 5 and 6).

The length data are better distributed after logarithmisation (Fig. 7 and 8). Conodont elements from the bedding planes are generally larger than those from the residues after the acid-dissolving method (Fig. 7), the same conclusion can be drawn when the elements are further divided into P, M, and S elements (Fig. 8). After removing the data of broken conodont elements, the violin plots of the length suggest that their distribution modes from the acid-dissolving method have been affected more than those from the bedding planes. This is reflected by positive skewness, flat kurtosis, and smaller mean and median sizes (Fig. 9).

#### 5. Discussion

Conodont elements are phosphatic micro-fossils (millimeter to micrometer) that belong to extinct marine crown vertebrates (Donoghue and Purnell, 1999; Goudemand et al., 2012). They were self-repairable if damaged when the conodont animals were alive, but they can be easily damaged after the death of the conodont animals and during extraction from the rock (von Bitter and Purnell, 2005). Furthermore, post-mortem conditions, such as sediment compaction and diagenesis, may differently bias the preservation of various elements in the apparatus (von Bitter and Purnell, 2005; Purnell and Donoghue, 2005).

The studied conodont elements were acquired from the Zhangjiawan section, which has been reported as a representative section for the Lower Triassic Nanzhang-Yuan'an Fauna (Yan et al., 2021). In this section, dark-colored lamellar limestones with abundant microbial-induced sediment



212

213

214

215

216

217

218

219

220

221

222

223

224

225

226

227

228

229

230

231

structures and marine reptile fossils are intercalated with massive dolomites and sandstones (Wu et al., 2023). The acquired conodont materials are from the middle part of the dark-colored lamellar limestone, which is also the thinnest bed of the Zhangjiawan section, suggesting that these conodont materials were deposited in a low-energy environment where sorting and selective destruction had only a slight influence on their preservations. However, the co-existence of conodont natural assemblages and isolated conodont elements on the bedding planes also may reflect that conodont elements experienced limited but non-negligible disturbances after their death. The ratios of different types of conodont elements from the bedding planes and the residues after acid-dissolving indicate that those elements have been affected by both natural and artificial processes (Table 1). On the one hand, elements show different resistances to post-mortem sorting, sediment compaction and diagenesis. As a special Early Triassic group with morphological similarity between their P1 and P2 elements, the conodont apparatus of Ellisonidae consists of 15 elements: four P elements, two M elements and nine S elements (Koike, 2016; Sun et al., 2020). However, the conodont elements analyzed in this study from the acid-dissolving method exhibit an enrichment of P elements or a shortage of M and S elements. This suggests that conodont elements are biasedly preserved even under low-energetic water, or that they may have been differently affected by lithification (Cooper et al., 2006; Sessa et al., 2009; Baets et al., 2022). For example, clusters of the earliest Triassic conodont *Hindeodus* indicated that their P<sub>2</sub> elements were more difficult to access or preserve even in a deep-water environment (see Zhang et al., 2017 and their comments by Agematsu et al., 2018). In shallow-water environments, stronger



233

234

235

236

237

238

239

240

241

242

243

244

245

246

247

248

249

250

251

252

hydrodynamics usually resulted in the depletion of all conodont elements except for the robust elements of Ellisonidae (Jiang et al., 2014; Wang et al., 2016). On the other hand, in our material, elements exhibited varying degrees of resistance to sorting during the laboratory process of the acid-dissolving method, often being broken. Compared to the conodont elements acquired from acid-dissolution, the ratio of S elements shows a significant decrease, while the ratio of M elements shows a slight or negligible decrease. This suggests that S elements have been more affected by the acid-dissolving method. Through isolated conodont elements obtained via the the aciddissolving method, Koike (2016) proposed the apparatus compositions of five species of Ellisonidae, and his materials also showed that their M and S elements were more readily (but not better) preserved than P elements (Fig. 3), although his results could have been obscured due to the differences in size and shape of conodont elements (Broadhead et al., 1990). The length distributions of conodont element from the two methods suggest that their preservation is affected by multiple factors (Table 1 and Fig. 8 and 9). Before being affected by the acid-dissolving process, M elements from the bedding-planes are smaller on average than P and S elements, while S elements are the largest among them. This is different from some reported well-preserved assemblages of Ellisonidae, which showed that P elements are smaller than M elements and that S elements are the largest (Sun et al., 2020), suggesting that M elements of Ellisonidae are more fragile than P elements. Additionally, research on the genus *Idiognathodus* showed that their S and M elements were usually larger than their P elements (see Fig. 4 in Purnell, 1993), which is consistent with Ellisonidae. As stated by Orchard (2005), conodont elements exhibited a higher representation of pectiniform elements (usually P elements) when they were



254

255

256

257

258

259

260

261

262

263

264

265

266

267

268

269

270

271

272

273

acquired from relatively nearshore, high-energy deposits where bias arising from post-mortem sorting and selective destruction cannot be ignored. This might be explained by element heterogeneity in mineralization or by their morphologies, as M elements are breviform digyrate and bear two inclined downward processes, while P elements are crescent-shaped angulate (Sun et al., 2020). S elements are smaller on average than P and M elements in the materials acquired from the acid-dissolving method, and the other types also show reductions in size by eliminating larger individuals (Fig. 8 and 9). This suggests that conodont elements are influenced by the method, potentially leading to breakage, even for the less vulnerable P elements. Notably, elements in the same position of different conodont species have variable endurances. For example, a Middle Triassic multi-element research of *Nicoraella germanica* indicated that P and M elements are over-represented (Table 1 in Chen et al., 2019). Previous studies have shown that the size of the conodont element is an ideal proxy for ecological changes (Balter et al., 2008; Luo et al., 2008; Chen et al., 2013; Leu et al., 2019; Wu et al., 2019; Zhang et al., 2020; Girard et al., 2023). For example, diametrical or harmonious sizechanging curves of conodont elements have been connected to transient or long-term ecological changes (Chen et al., 2013; Ginot and Goudemand, 2019; Zhang et al., 2020). However, conodont elements may exhibit different size variation trends during the same interval (Leu et al., 2019). This might result from their different response mechanisms, which are further connected to their different habitats (Joachimski et al., 2012; Sun et al., 2012; Leu et al., 2019; Chen et al., 2021). Although the size of conodont element can be controlled by ecological factors, and bias from laboratory processes has a limited impact on conclusions during conodont apparatus



reconstructions (Chen et al., 2016), it is still worth noticing that different degrees of influences may occur when data are used for different aims (Jeppsson, 2005). This study showed that conodont elements might have experienced different degrees of artificial damage during laboratory processes. Therefore, attention must be paid when trying to decipher conodont data for taxonomy, ecology, and other purposes, especially when conodont species have variant morphology of multi-elements.

#### 6. Conclusions

Conodont elements (including clusters) (Ellisonidae) from the bedding planes of the Early Triassic Nanzhang-Yuan'an Lagerstätte, as well as conodont elements acquired from the corresponding bed through the acid-dissolving method, provide insight into the biases that must be taken in account when deciphering conodont materials. Conodont elements from both methods exhibit varying degrees of bias, especially those from the acid-dissolving method, which introduces additional bias beyond that inherent to the bedding-plane materials. Owing to their different tolerances caused by different morphologies, conodont elements of Ellisonidae in different positions exhibit selective preservation or varing degrees of destruction even before laboratory processes. The widely used acid-dissolving method increases the bias by selectively destroying the M and S elements. Large individuals of all three different elements are prone to breaking during laboratory processing, with S elements being the most affected. This study indicates that biases in the size and morphology of conodonts caused by natural and artificial laboratory processes must be considered when deciphering these data.



295	
296	Acknowledgments
297	SEM pictures were taken at the State Key Laboratory of Biogeology and Environmental
298	Geology in China University of Geosciences.
299	
300	Conflict of interest The authors declare that they have no conflict of interest.
301	
302	References
303	Agematsu, S., Golding, M.L., Orchard, M.J., 2018. Comments on: testing hypotheses of element
304	loss and instability in the apparatus composition of complex conodonts (Zhang et al.).
305	Palaeontology 61, 785–792.
306	Aldridge, R.J., Briggs, D.E.G., Smith, M.P., Clarkson, E.N.K., Clark, N.D., 1993. The anatomy
307	of conodonts. Philosophical Transactions of the Royal Society of London. Series B:
308	Biological Sciences, 1993, 340.1294: 405–421.
309	Baets, K.D., Klug, C., Korn, D., Landman, N.H., 2012. Early evolutionary trends in ammonoid
310	embryonic development. Evolution 66, 1788–1806.
311	Baets, K.D., Jarochowska, E., Buchwald, S.Z., Klug, C., Korn, D., 2022. Lithology controls
312	ammonoid size distributions. Palaios 37, 744-754.
313	Balter, V., Renaud, S., Girard, C., Joachimski, M.M., 2008. Record of climate-driven
314	morphological changes in 376 Ma Devonian fossils. Geology 36, 907-910.
315	Benton, M.J., Zhang, Q.Y., Hu, S.X., Chen, Z.Q., Wen, W., Liu, J., Huang, J.Y., Zhou. C.Y.,



316	Xie, T., Tong, J.N., Choo, B., 2013. Exceptional vertebrate biotas from the Triassic of
317	China, and the expansion of marine ecosystems after the Permo-Triassic mass extinction
318	Earth-Science Reviews 125, 199–243.
319	Briggs, D.E., Clarkson, E.N., Aldridge, R. J., 1983. The conodont animal. Lethaia, 16(1), 1–14.
320	Broadhead, T.W., Driese, S.G., Harvey, J.L., 1990. Gravitational settling of conodont elements:
321	Implications for paleoecologic interpretations of conodont assemblages. Geology 18,
322	850–853.
323	Chen, Y.L., Joachimski, M.M., Richoz, S., Krystyn, L., Aljinovi'c, D., Smirčić, D., Kolar-
324	Jurkov sek, T., Lai, X.L., Zhang, Z.F., 2021. Smithian and Spathian (Early Triassic)
325	conodonts from Oman and Croatia and their depth habitat revealed. Global and Planetar
326	Change, 196, 103362.
327	Chen, Y.L., Twitchett, R.J., Jiang, H.S., Richoz, S., Lai, X.L., Yan, C.B., Sun, Y.D., Liu, X.D.,
328	Wang, L.N., 2013. Size variation of conodonts during the Smithian-Spathian (Early
329	Triassic) global warming event. Geology 41, 823-826.
330	Chen, Y., Krystyn, L., Orchard, M. J., Lai, X. L., Richoz, S., 2016. A review of the evolution,
331	biostratigraphy, provincialism and diversity of M iddle and early L ate T riassic
332	conodonts. Papers in Palaeontology, 2(2), 235–263.
333	Chen, Y.L., Neubauer, T.A., Krystyn, L., Richoz, S., 2016. Allometry in Anisian (Middle
334	Triassic) segminiplanate conodonts and its implications for conodont taxonomy.
335	Palaeontology 59, 725–741.
336	Chen, Y.L., Scholze, F., Richoz, S., Zhang, Z.F., 2019. Middle Triassic conodont assemblages



from the Germanic Basin: implications for multi-element taxonomy and biogeography. 337 Journal of Systematic Palaeontology 17, 359–377. 338 Clark, D.L., 1983. Extinction of conodonts. Journal of Paleontology 57, 652–661. 339 Cooper, R.A., Maxwell, P.A., Crampton, J.S., Beu, A.G., Jones, C.M., Marshall, B. A., 2006. 340 Completeness of the fossil record: estimating losses due to small body size. Geology 34, 341 342 241-244. Dal Corso, J., Song, H., Callegaro, S., Chu, D., Sun, Y., Hilton, J., Grasby, S. E., Joachimski, M. 343 M., Wignall, P. B., 2022. Environmental crises at the Permian–Triassic mass extinction. 344 Nature Reviews Earth & Environment 3, 197–214. 345 Du, Y.X., Chiari, M., Karádi, V., Nicora, A., Onoue, T., Pálfy, J., Roghi, G., Tominmatsu, Y., 346 Rigo, M., 2020. The asynchronous disappearance of conodonts: New constraints from 347 Triassic-Jurassic boundary sections in the Tethys and Panthalassa. Earth-Science 348 Reviews 203, 103176. 349 Donoghue, P.C., Purnell, M.A., 1999. Growth, function, and the conodont fossil record. Geology 350 27, 251-254. 351 Gabbott, S.E., Aldridge, R.J., Theron, J.N., 1995. A giant conodont with preserved muscle tissue 352 from the Upper Ordovician of South Africa. Nature 374, 800–803. 353 Ginot, S., Goudemand, N., 2019. Conodont size, trophic level, and the evolution of platform 354 elements. Paleobiology 45, 458-468. 355 Girard, C., Charruault, A. L., Dufour, A. B., Renaud, S., 2023. Conodont size in time and space: 356 Beyond the temperature-size rule. Marine Micropaleontology 184, 102291. 357



358	Goudemand, N., Orchard, M.J., Urdy, S., Bucher, H., Tafforeau, P., 2011. Synchrotron-aided
359	reconstruction of the conodont feeding apparatus and implications for the mouth of the
360	first vertebrates. Proceedings of the National Academy of Sciences, 108, 8720-8724.
361	Goudemand, N., Orchard, M.J., Tafforeau, P., Urdy, S., Brühwiler, T., Brayard, A., Galfetti, T.,
362	Bucher, H., 2012. Early Triassic conodont clusters from South China: revision of the
363	architecture of the 15 element apparatuses of the superfamily Gondolelloidea.
364	Palaeontology 55, 1021-1034.
365	Jeppsson, L., Anehus, R., 1995. A buffered formic acid technique for conodont extraction.
366	Journal of Paleontology 69, 790–794.
367	Jeppsson, L., 2005. Biases in the recovery and interpretation of micropalaeontological data.
368	Special Papers in Palaeontology, 73, 57–71.
369	Jiang, H.S., Lai, X.L., Luo, G.M., Aldridge, R., Zhang, K.X., Wignall, P., 2007. Restudy of
370	conodont zonation and evolution across the P/T boundary at Meishan section, Changxing
371	Zhejiang, China. Global and Planetary Change, 55, 39-55.
372	Jiang, H.S., Lai, X.L., Sun, Y.D., Wignall, P.B., Liu, J.B., Yan, C.B., 2014. Permian Triassic
373	conodonts from Dajiang (Guizhou, South China) and their Implication for the age of
374	microbialite deposition in the aftermath of the end-Permian Mass Extinction. Journal of
375	Earth Science, 25, 413–430.
376	Joachimski, M.M., Lai, X.L., Shen, S.Z., Jiang, H.S., Luo, G.M., Chen, B., Chen, J., Sun, Y.D.,
377	2012. Climate warming in the latest Permian and the Permian–Triassic mass extinction.
378	Geology 40, 195–198.



Koike, T., 2016. Multielement conodont apparatuses of the Ellisonidae from Japan. 379 Paleontological Research 20, 161–175. 380 Kimming, J., Schiffbauer, J.D., 2024. A modern definition of Fossil-Lagerstätten. Trends in 381 Ecology & Evolution. In press. 382 Luo, G.M., Lai, X.L., Shi, G.R., Jiang, H.S., Yin, H.F., Xie, S.C., Tong, J.N., Zhang, K.X., He, 383 384 W.H., Wignall, P.B., 2008. Size variation of conodont elements of the *Hindeodus*– Isarcicella clade during the Permian-Triassic transition in South China and its 385 implication for mass extinction. Palaeogeography, Palaeoclimatology, Palaeoecology 386 264, 176-187. 387 Leu, M., Bucher, H., Goudemand, N. 2019. Clade-dependent size response of conodonts to 388 environmental changes during the late Smithian extinction. Earth-Science Reviews 195, 389 390 52-67. Martínez-Pérez, C., Plasencia, P., Cascales-Miñana, B., Mazza, M., Botella, H., 2014. New 391 insights intsuno the diversity dynamics of Triassic conodonts. Historical Biology 26, 392 591-602. 393 Martínez-Pérez, C., Cascales-Miñana, B., Plasencia, P., Botella, H., 2015. Exploring the major 394 depletions of conodont diversity during the Triassic. Historical Biology 27, 503–507. 395 Orchard, M.J., 2005. Multielement conodont apparatuses of Triassic Gondolelloidea: Conodont 396 biology and phylogeny: interpreting the fossil record. Special Papers in Palaeontology 73. 397 73-101. 398 Orchard, M.J., 2007. Conodont diversity and evolution through the latest Permian and Early 399



400 Triassic upheavals: Palaeogeography, Palaeoclimatology, Palaeoecology 252, 93–117. Purnell, M.A., 1993. Feeding mechanisms in conodonts and the function of the earliest vertebrate 401 hard tissues. Geology 21, 375-377. https://doi/10.1130/0091-402 7613(1993)021<0375:FMICAT>2.3.CO;2. 403 Purnell, M.A., Donoghue, P.C., Aldridge, R.J., 2000. Orientation and anatomical notation in 404 405 conodonts. Journal of Paleontology 74, 113-122. Purnell, M.A., Donoghue, P.C., 2005. Between death and data: biases in interpretation of the 406 fossil record of conodonts. Special Papers in Palaeontology 73, 7–25. 407 Raup, D.M., 1991. The future of analytical paleobiology. Short Courses in Paleontology 4. 408 207–216. Sessa, J.A., Patzkowsky, M.E., Bralower, T.J., 2009. The impact of lithification 409 on the diversity, size distribution, and recovery dynamics of marine invertebrate 410 assemblages. Geology 37, 115-118. 411 Rigo, M., Onoue, T., Wu, Q.W., Tomimatsu, Y., Santello, L., Du, Y.X., Jin, X., Bertinelli, A., 412 2023. A new method for extracting conodonts and radiolarians from chert with NaOH 413 solution. Palaeontology 66, e12672. 414 Sansom, I.J., Smith, M.P., Armstrong, H.A., Smith, M.M., 1992. Presence of the earliest 415 vertebrate hard tissue in conodonts. Science 256, 1308–1311. 416 Shen, S.Z., 2023. The Permian GSSPs and timescale: Progress, unsolved problems and 417 perspectives. Permophiles 75, 12–18. 418 Sun, Y.D., Joachimski, M.M., Wignall, P.B., Yan, C.B., Chen, Y.L., Jiang, H.S., Wang, L.N., 419 Lai, X.L., 2012. Lethally hot temperatures during the Early Triassic greenhouse. Science 420

421	338, 366–370.
422	Sun, Z.Y., Liu, S., Ji, C., Jiang, D.Y., Zhou, M., 2020. Synchrotron-aided reconstruction of the
423	prioniodinin multielement conodont apparatus (Hadrodontina) from the Lower Triassic
424	of China. Palaeogeography, Palaeoclimatology, Palaeoecology 560, 109913.
425	Takahashi, S., Yamakita, S., & Suzuki, N., 2019. Natural assemblages of the conodont Clarkina
426	in lowermost Triassic deep-sea black claystone from northeastern Japan, with probable
427	soft-tissue impressions. Palaeogeography, Palaeoclimatology, Palaeoecology, 524,
428	212–229.
429	Von Bitter, P. H. 1972. Environmental control of conodont distribution in the Shawnee Group
430	(Upper Pennsylvanian) of eastern Kansas. University of Kansas Paleontological
431	Contributions 59, 105 p.
432	von Bitter, H.P., Purnell, M.A., 2005. An experimental investigation of post-depositional
433	taphonomic bias in conodonts. Special Papers in Palaeontology 73, 39-56.
434	Wang, L., Sun, Y., Wigall, P.B., Xing, A., Chen, Z.X., Lai, X.L., 2023. The Permian-Triassic
435	Merrillina (conodont) in South China and its ecological significance. Marine
436	Micropaleontology, 180, 102228.
437	Wu, K., Tian, L., Liang, L., Metcalfe, I., Chu, D.L., Tong, J.N., 2019. Recurrent biotic rebounds
438	during the Early Triassic: biostratigraphy and temporal size variation of conodonts from
439	the Nanpanjiang Basin, South China. Journal of the Geological Society 176, 1232-1246.
440	Wu, K., Zou, Y.R., Li, H.J., Wan, S., Yang, L.Z., Cui, Y.S., Li, J.L., Zhao, B., Cheng, L., 2023.
441	A unique early Triassic (Spathian) conodont community from the Nanzhang-Yuan'an



442	Fauna, Hubei Province, South China. Geological Journal 58, 3879–3898.
443	Yan, C.B., Li, J.L., Cheng, L., Zhao, B., Zou, Y.R., Niu, D.Y., Chen, G., Fang, Z.H., 2021.Strata
444	characteristics of the Early Triassic Nanzhang-Yuan'an Fauna in Western Hubei
445	Province. Journal of Earth Science 46, 122–135.
446	Zhang, M.H., Jiang, H.S., Purnell, M. A., Lai, X.L., 2017. Testing hypotheses of element loss
447	and instability in the apparatus composition of complex conodonts: articulated skeletons
448	of <i>Hindeodus</i> . Palaeontology 60, 595–608.
449	Zhang, X.S., Li, S.Y., Song, Y.F., Gong, Y.M 2020, Size reduction of conodonts indicates high
450	ecological stress during the late Frasnian under greenhouse climate conditions in South
451	China. Palaeogeography, Palaeoclimatology, Palaeoecology 556, 109909.
452	Zhao, L.S., Chen, Y.L., Chen, Z.Q., Cao, L., 2013, Uppermost Permian to Lower Triassic
453	conodont zonation from Three Gorges area, South China. Palaios 28, 523-540.
454	
455	
456	Table 1. Number, ratio, length range, length average of conodont elements and their
457	differences.
458	
459	Figure 1. Conodont elements recovered from Zhangjiawan section, Yuan'an County, Hubei
460	Province, South China. (A) Dark-colored laminated limestone of the uppermost Jialingjiang
461	Formation. The dashed line indicates the thinnest beds where the clusters were found. (B)
462	Recovered conodont cluster after acetic acid dissolution. (C) Isolated conodont element



463	found from the bedding plane. (D, E and F) Conodont natural assemblage found from the
464	bedding plane. (G-N) Different isolated elements and clusters found from the bedding plane.
465	(Also see the supplementary material of Wu et al., 2023). Photo credit: Kui Wu.

Figure 2. Differences between the standard composition of the Ellisonidae apparatus and the materials form this study. (A) Radar chart depicting the percentage of different conodont elements from the bedding planes, the acid-dissolution method, and the standard composition of the Ellisonidae apparatus. (B) Difference chart illustrating variations in conodont elements from the bedding planes, the acid-dissolution method, and the standard composition of the Ellisonidae apparatus. The y-axis represents the percentage change of different elements relative to the Reference (the standard component of the *Ellisonia* apparatus)

Figure 3. Ratios of different conodont elements from this study and Koike (2016) compared to the standard composition of the Ellisonidae apparatus. Refer. represents the standard component of the Ellisonia apparatus. Error bars represent 95% binomial confidence intervals (Raup 1991; Baets et al., 2012). A-I are data from Koike (2016). A represents Hadrodontina aequabilis (sample A), B represents Hadrodontina aequabilis (sample B), C represents Hadrodontina aequabilis (sample C), D represents Ellisonia triassica, E represents Corudina breviramulis, F represents Staeschegnathus perrii (sample A), G represents Staeschegnathus perrii (sample A), G represents



184	conodonts of Kolke (2016), J represents bedding plane conodont elements of this study, K
185	represents conodont elements from acid-dissolution of this study, L represents the standard
186	component of the Ellisonia apparatus (Confidence intervals are not used here because only
187	one apparatus is available).
188	
189	Figure 4. Comparison of complete and broken conodont elements from the bedding planes
190	and the acid-dissolving method. (A) Numbers of different elements. (B). Ratios of different
191	elements. Error bars represent 95% binomial confidence intervals (Raup 1991; Baets et al.,
192	2012).
193	
194	Figure 5. Histograms of the length of all conodont elements from the bedding planes and the
195	acid-dissolution method. The dark-black represent conodont elements from the bedding
196	planes; the grey-black represent conodont elements from the acid-dissolution method. (A)
197	All elements. (B) P elements. (C) M elements. (D) S elements.
198	
199	Figure 6. Length distributions (logarithmized with base 10) of complete and broken conodont
500	elements from the bedding planes and the acid-dissolution method. The black dots represent
501	complete conodont elements; the green dots represent broken conodont elements. (A) All
502	elements; (B) M elements; (C) P elements; (D) S elements.
503	

Figure 7. Distributions of length (after logarithmisation) for all conodont elements from the

504





505	bedding planes and residues after acid-dissolving. (A) Distributions of length. (B) Quantile-
506	Quantile plot of the length.
507	
808	Figure 8. Distributions of length (after logarithmisation) for different conodont elements
509	from the bedding planes and residues after acid-dissolving. The dark dots represent data
510	from the bedding planes. The grey dots represent data from the acid-dissolving method. (A)
511	Distributions of length of P elements. (B) Distributions of length of M elements. (C)
512	Distributions of length of S elements. (D) Violin-plot of different conodont elements.
513	
514	Figure 9. Violin-plot of length of completely preserved conodont elements.
515	



#### Figure 1

Conodont elements recovered from Zhangjiawan section, Yuan'an County, Hubei Province, South China. (A) Dark-colored laminated limestone of the uppermost Jialingjiang Formation. The dashed line indicates the thinnest beds where the clusters were found. (B) Recovered conodont cluster after acetic acid dissolution. (C) Isolated conodont element found from the bedding plane. (D, E and F) Conodont natural assemblage found from the bedding plane. (G-N) Different isolated elements and clusters found from the bedding plane. (Also see the supplementary material of Wu et al., 2023). Photo credit: Kui Wu.

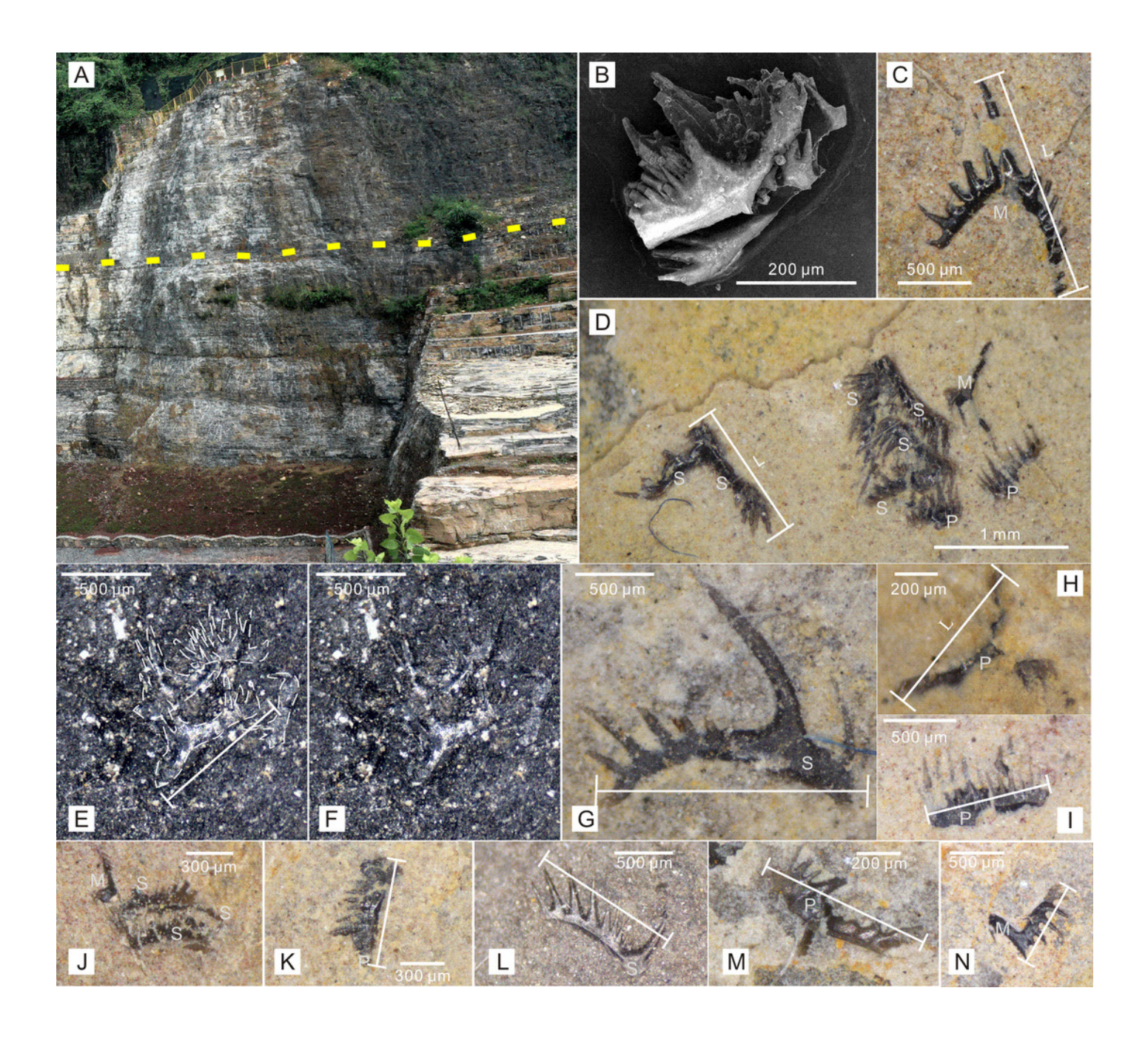




#### Figure 2

Differences between the standard composition of the Ellisonidae apparatus and the materials form this study. (A) Radar chart depicting the percentage of different conodont elements from the bedding planes, the acid-dissolution method, and the standard composition of the Ellisonidae apparatus. (B) Difference chart illustrating variations in conodont elements from the bedding planes, the acid-dissolution method, and the standard composition of the Ellisonidae apparatus. The y-axis represents the percentage change of different elements relative to the Reference (the standard component of the Ellisonia apparatus)

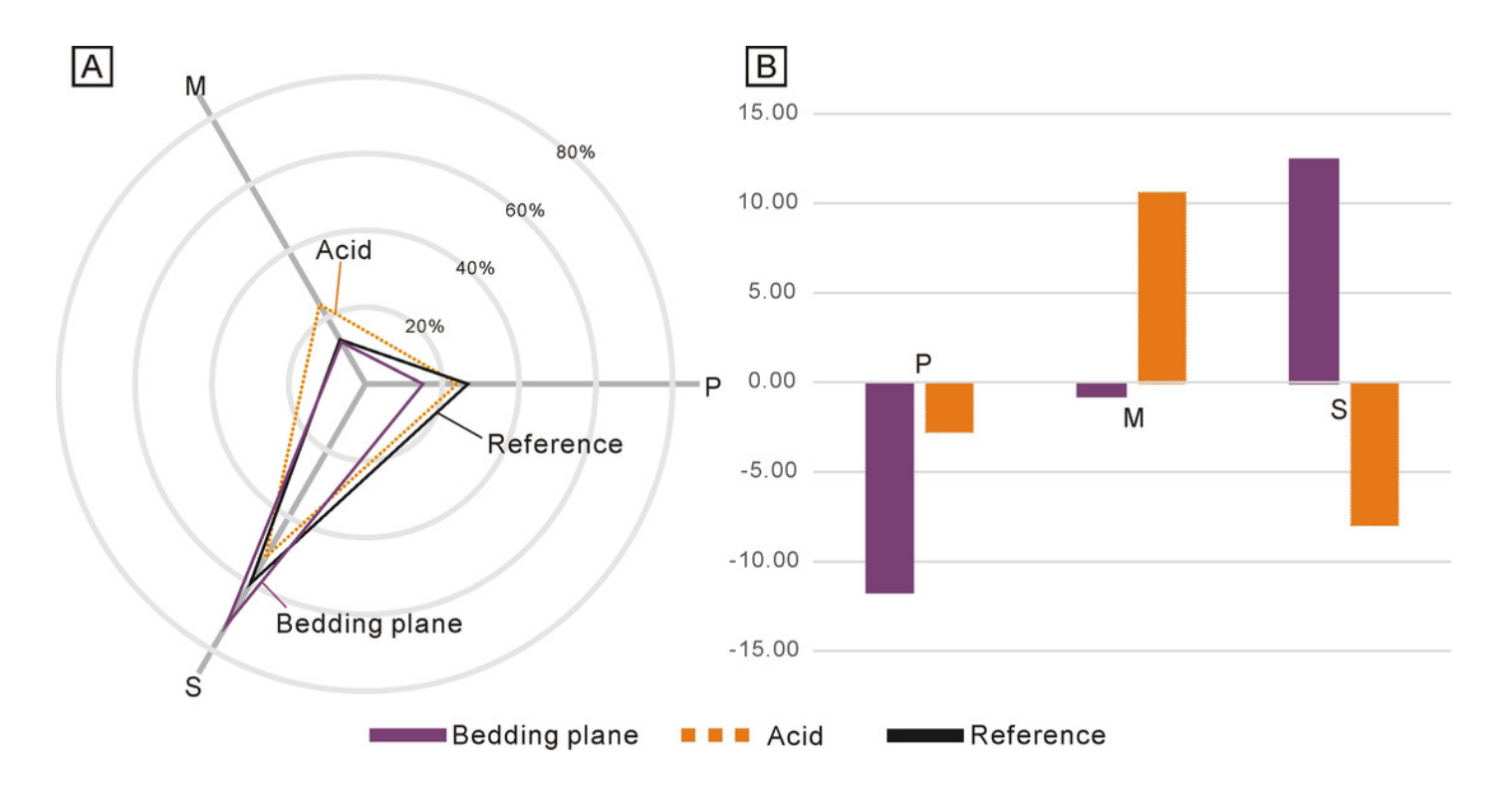


#### Figure 3

Ratios of different conodont elements from this study and Koike (2016) compared to the standard composition of the Ellisonidae apparatus. Refer. represents the standard component of the Ellisonia apparatus. Error bars represent 95% binomial confidence intervals (Raup 1991; Baets et al., 2012). A-I are data from Koike (2016). A represents Hadrodontina aequabilis (sample A), B represents Hadrodontina aequabilis (sample B), C represents Hadrodontina aequabilis (sample C), D represents Ellisonia triassica, E represents Corudina breviramulis, F represents Staeschegnathus perrii (sample A), G represents Staeschegnathus perrii (sample B), H represents Furnishius triserratus, I represents all the conodonts of Koike (2016), J represents bedding plane conodont elements of this study, K represents conodont elements from acid-dissolution of this study, L represents the standard component of the Ellisonia apparatus (Confidence intervals are not used here because only one apparatus is available).



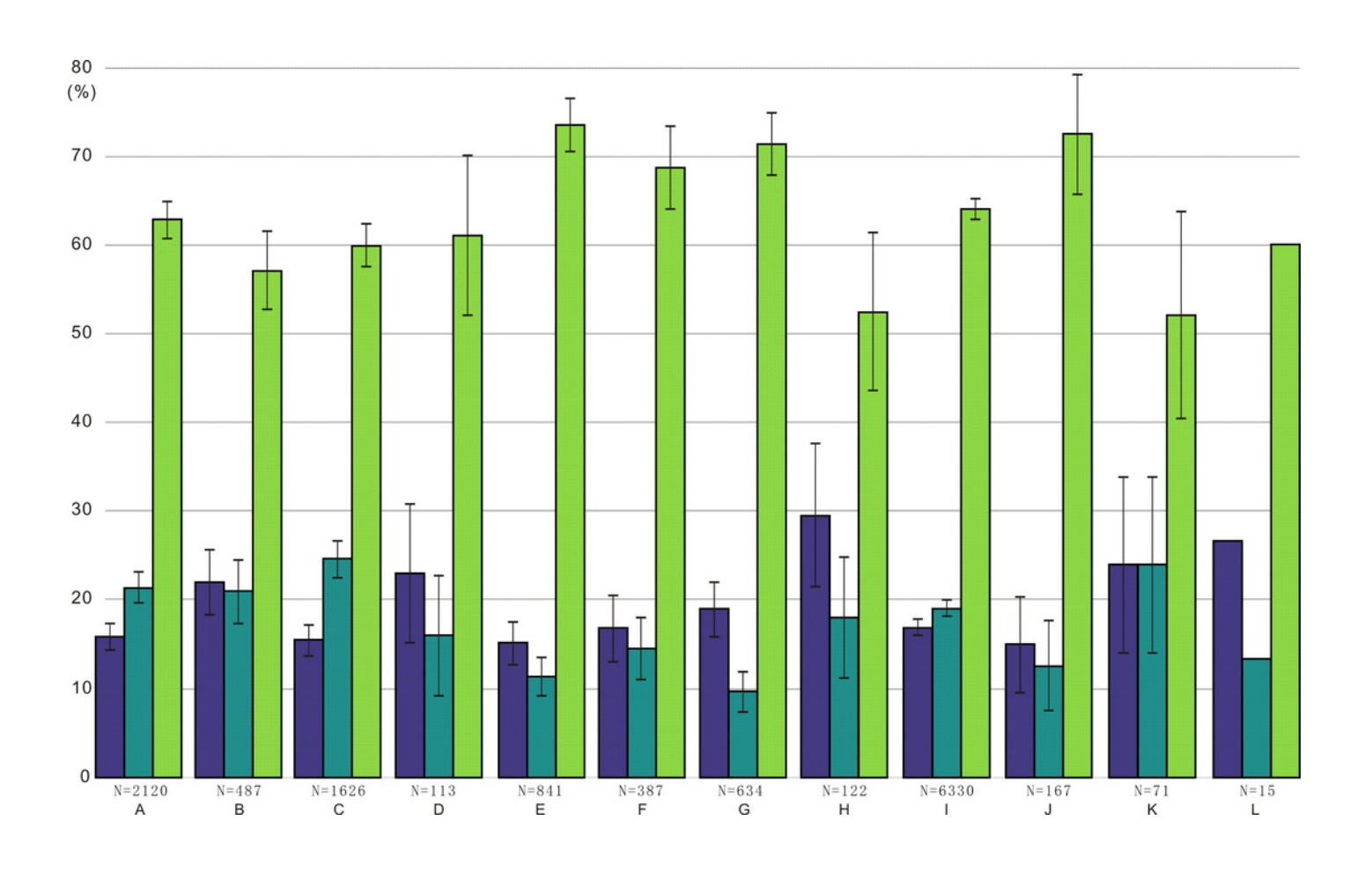
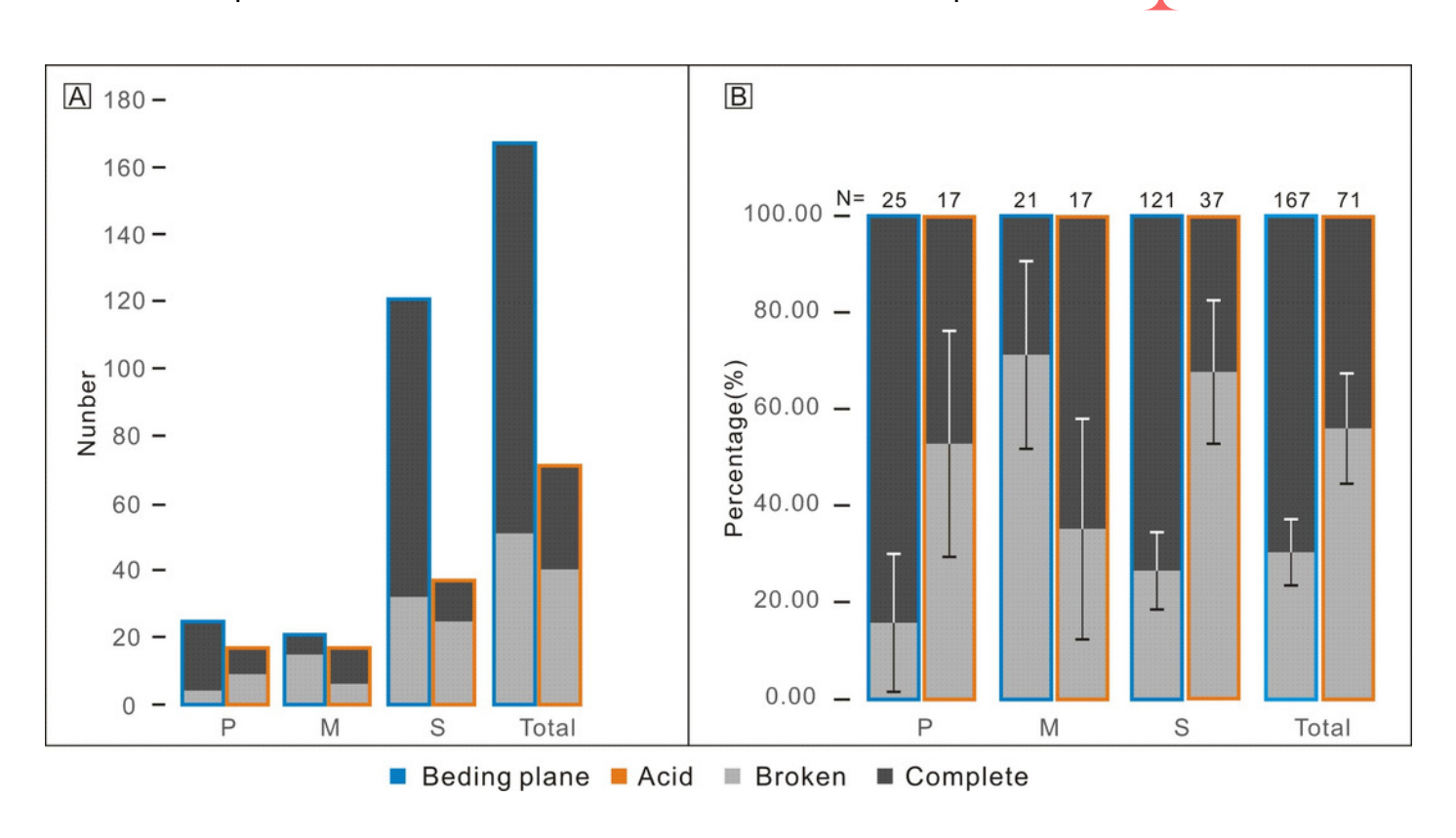




Figure 4

Comparison of complete and broken conodont elements from the bedding planes and the acid-dissolving method. (A) Numbers of different elements. (B). Ratios of different elements. Error bars represent 95% binomial confidence intervals (Raup 1991; Baets et al., 2012).



### Figure 5

Histograms of the length of all conodont elements from the bedding planes and the acid-dissolution method. The dark-black represent conodont elements from the bedding planes; the grey-black represent conodont elements from the acid-dissolution method. (A) All elements. (B) P elements. (C) M elements. (D) S elements.

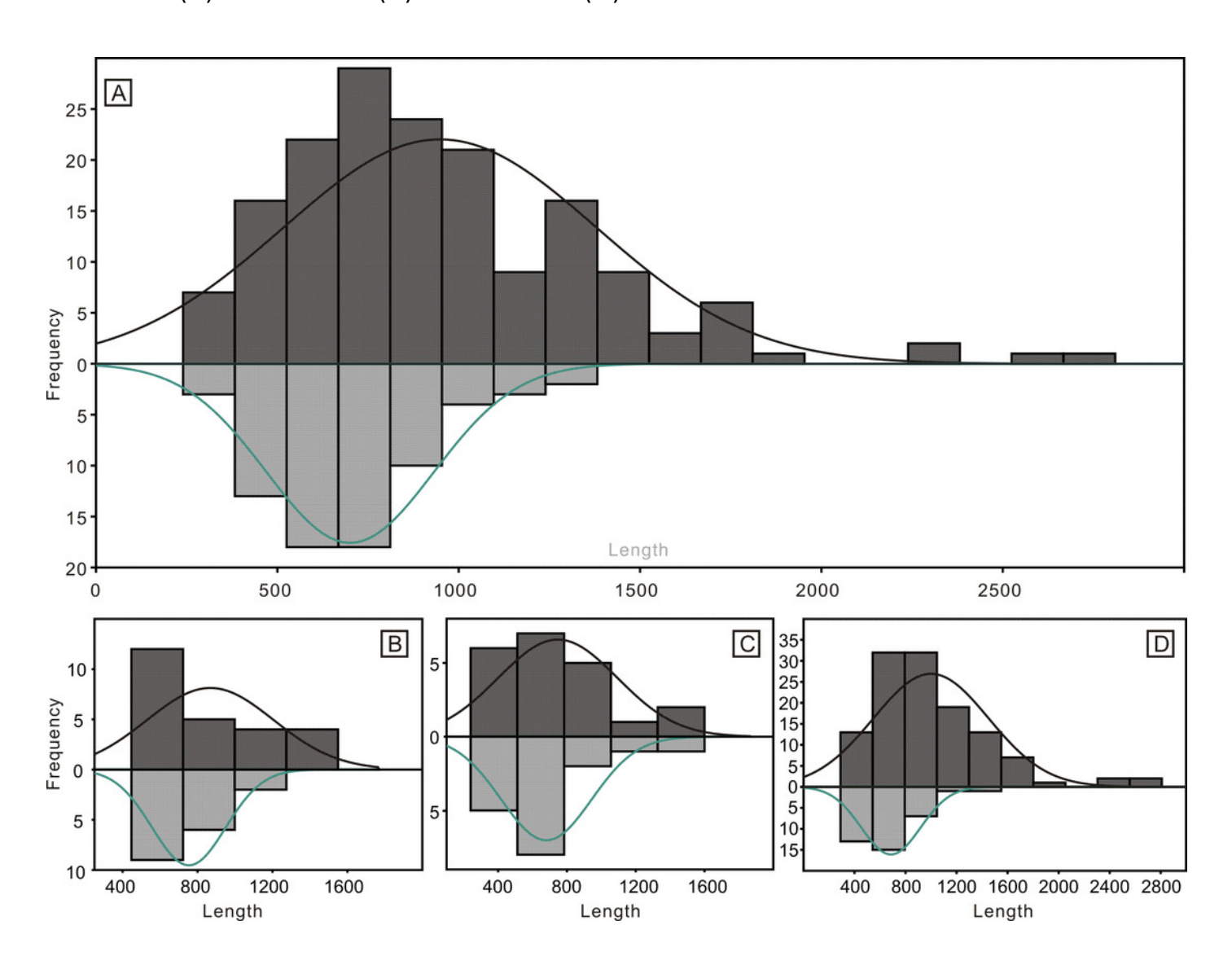




### Figure 6

Length distributions (logarithmized with base 10) of complete and broken conodont elements from the bedding planes and the acid-dissolution method. The black dots represent complete conodont elements; the green dots represent broken conodont elements. (A) All elements; (B) M elements; (C) P elements; (D) S elements.



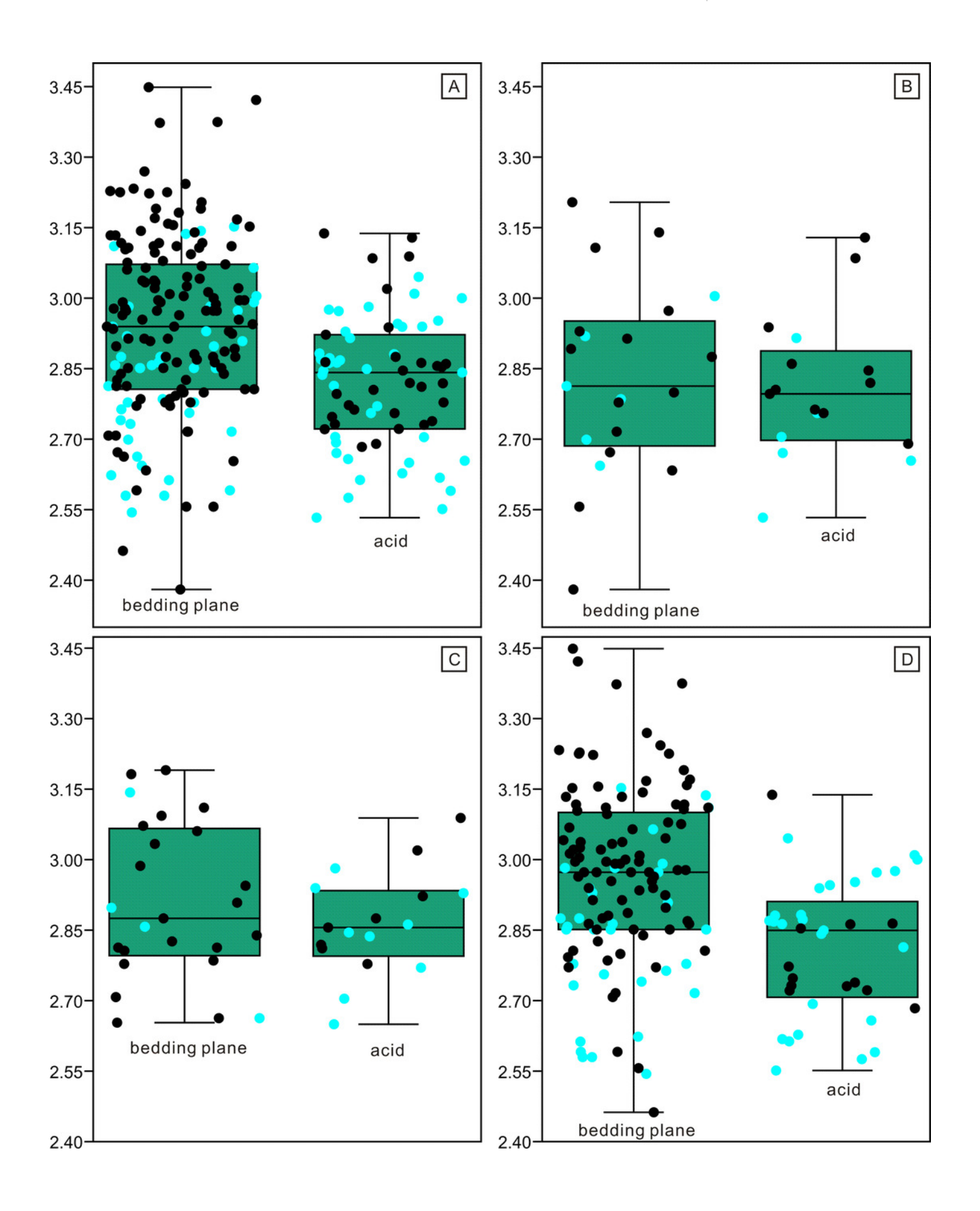




### Figure 7

Distributions of length (after logarithmisation) for all conodont elements from the bedding planes and residues after acid-dissolving. (A) Distributions of length. (B) Quantile-Quantile plot of the length.



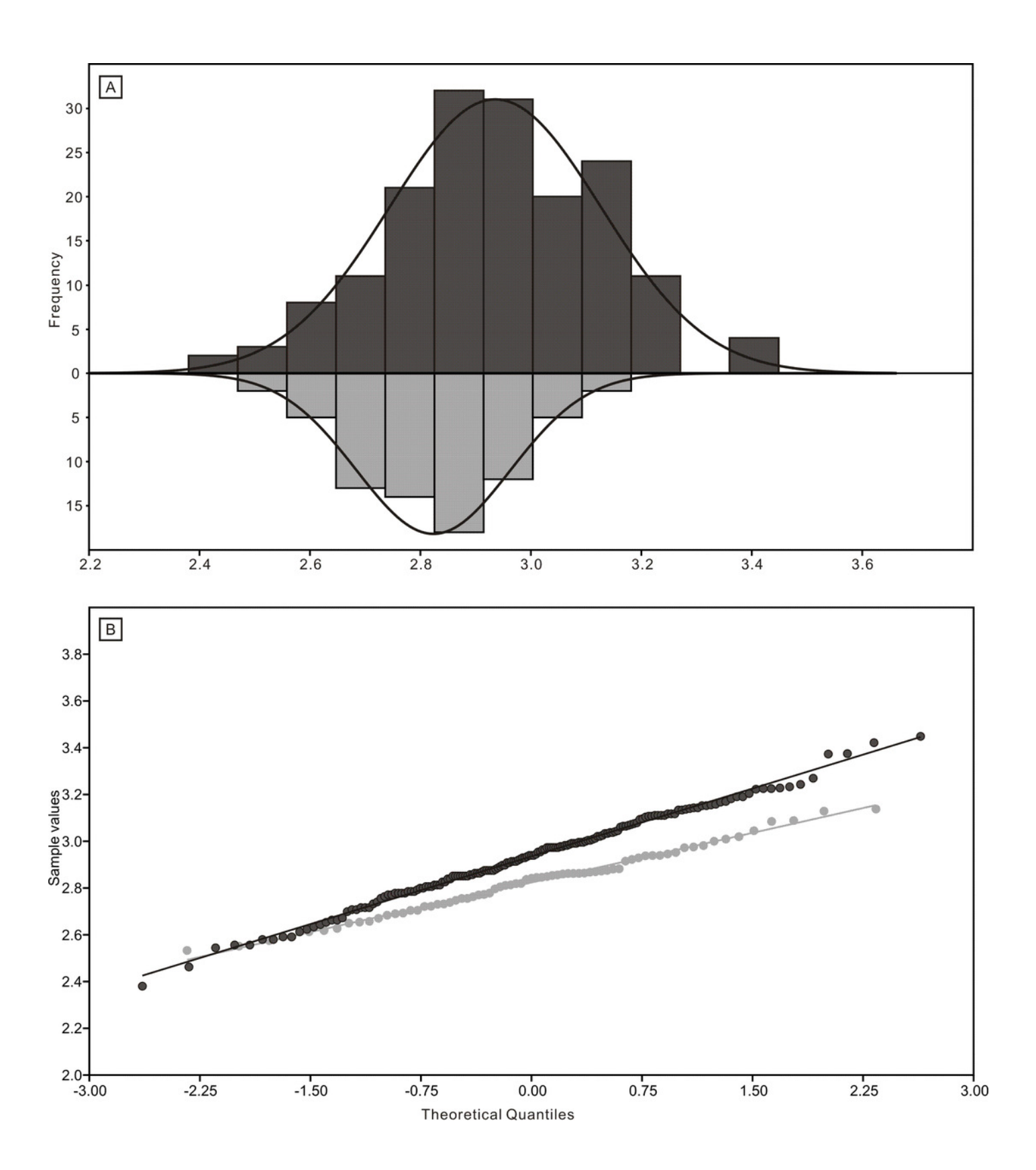




#### Figure 8

Distributions of length (after logarithmisation) for different conodont elements from the bedding planes and residues after acid-dissolving. The dark dots represent data from the bedding planes. The grey dots represent data from the acid-dissolving method. (A) Distributions of length of P elements. (B) Distributions of length of M elements. (C) Distributions of length of S elements. (D) Violin-plot of different conodont elements.

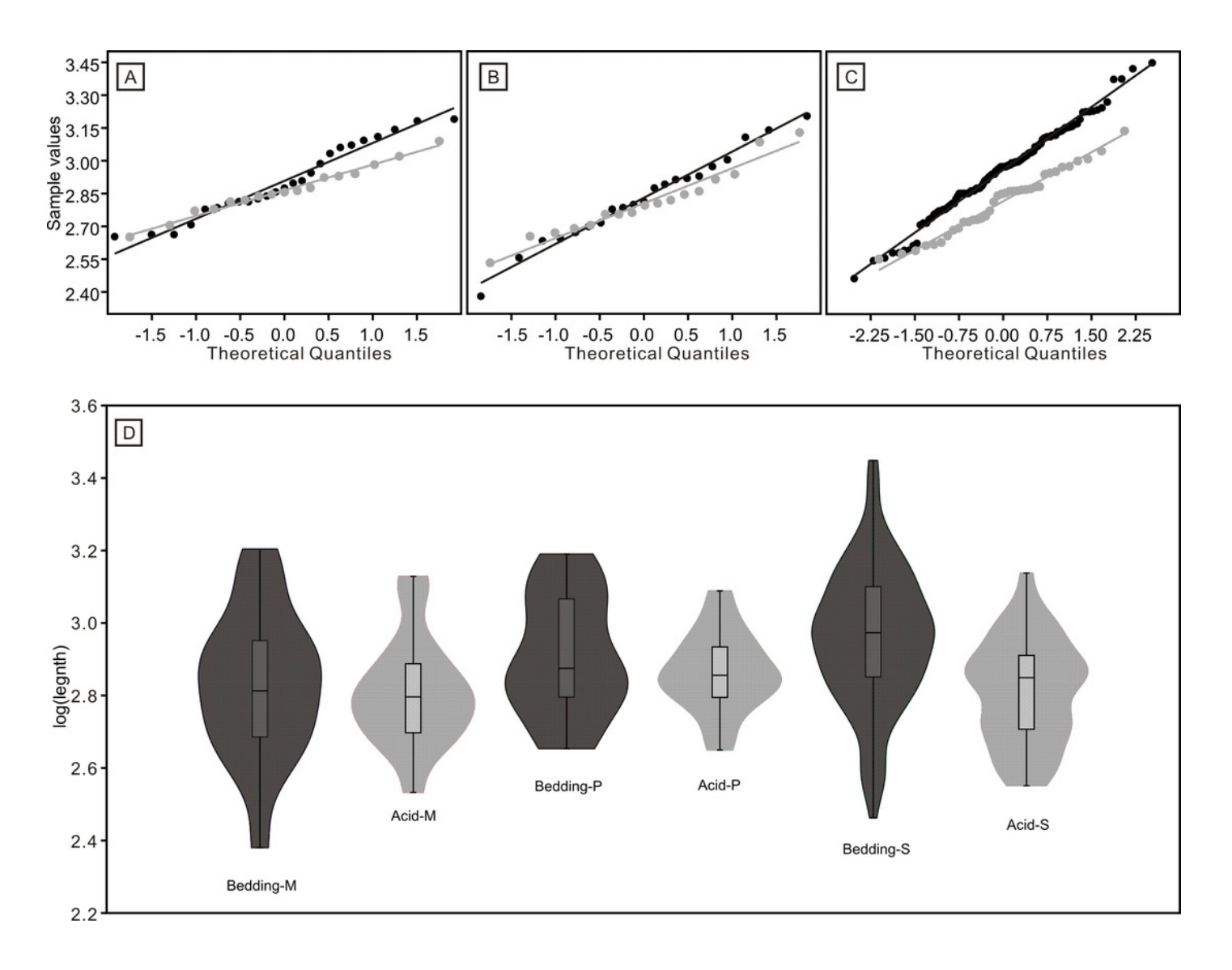
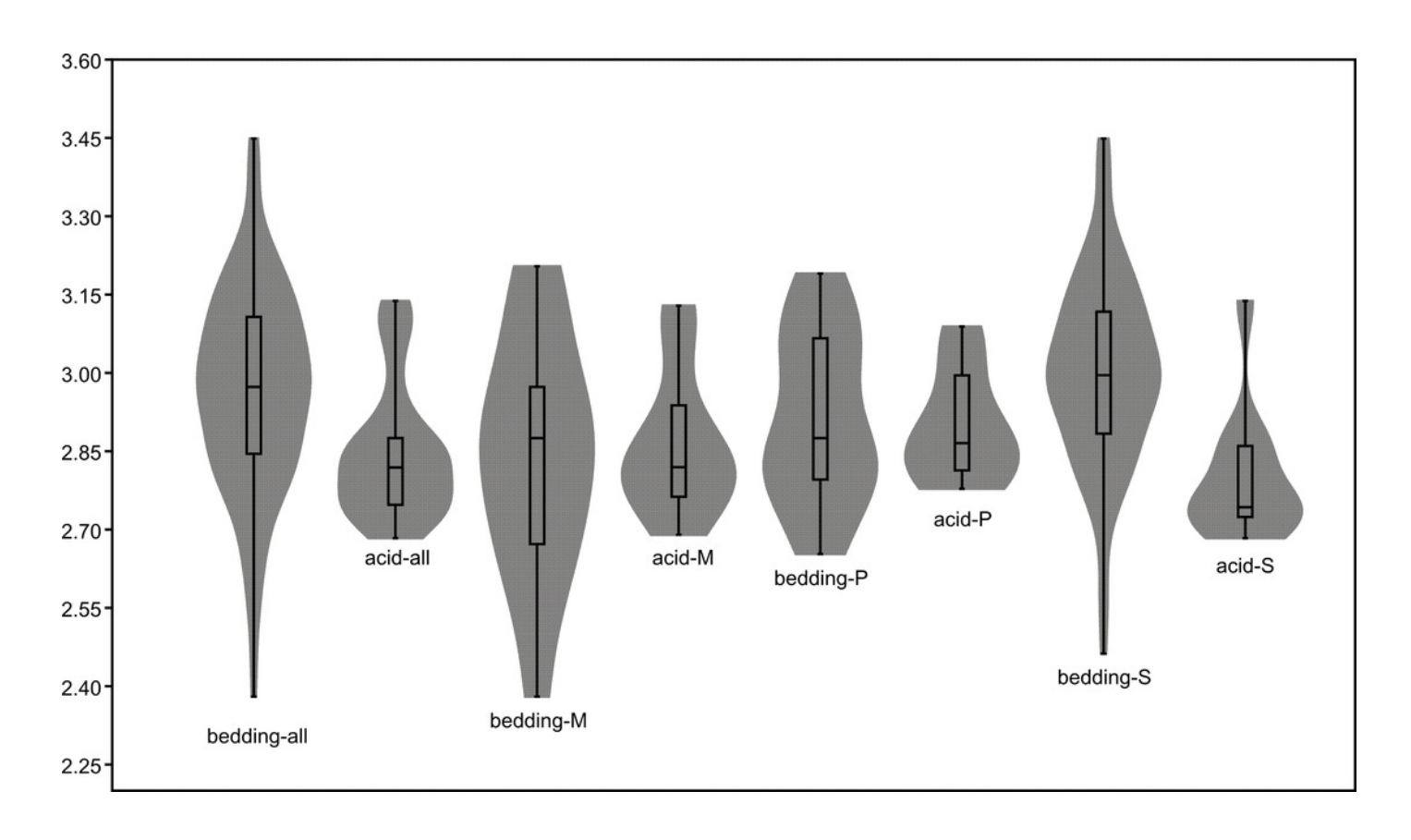




Figure 9

Violin-plot of length of completely preserved conodont elements.





### Table 1(on next page)

Table 1

Number, ratio, length range, length average of conodont elements and their differences.

Table 1. Number, ratio, length range, length average of conodont elements and their differences.

	Position/type		Р	Complete (N/P)	Broken (N/P)	Material/	R	A	S	A*	S*			
Acquiring		N				Original	(µm)	(µm)	(µm)	(µm)	(µm)	p	<i>p</i> *	
way		IV.				Ratio								
						(P:M:S)								
	P	25	#####	21/84.00%	4/16.00%		450~1550	868.4	332			0.21		
Bedding	M	21	#####	6/28.57%	15/71.43%	1.2:1:5.8/	240~1600	747.1	338	948	430.6	0.51	< 0.01	
Planes	S 12	121	121 #####	89/73.55%	32/26.45%	2:1:4.5	290~	999.9	000.0	450	948	430.0	<0.01	<0.01
		121					2810		450			< 0.01		
	P	17	#####	8/47.06%	9/52.94%	1.1.2.2/	447~1226	753.8	190			0.21		
Disolution	M	17	#####	11/64.71%	6/35.29%	1:1:2.2/	341~1345	680.8	255	701	228.5	0.51	< 0.01	
	S	37	#####	12/32.43%	25/67.57%	2:1:4.5	356~1373	685.5	228			< 0.01		

Note: N-Number of speciemens; P-Percentage; R-Range of length; A—Average of length; A\*—Average of length (all elements); p-p-Value for the t-tests(contrast with the same type);  $p^*-p$ -Value for the t-tests(contrast with all elements); S—stantard deviation